Small-angle neutron-scattering investigation of long-range correlations in silica aerogels: Simulations and experiments

Anwar Hasmy, Eric Anglaret, Marie Foret, Jacques Pelous, and Rémi Jullien
Laboratoire de Science des Matériaux Vitreux, Université Montpellier II, Place Eugène Bataillon, 34095 Montpellier Cedex 5, France
(Received 6 December 1993; revised manuscript received 13 April 1994)

Numerical simulations of gel formation by off-lattice diffusion-limited cluster-cluster aggregation (DLCA) of identical spherical particles in a cubic box are performed. Both the correlation function $g(r)$ and the small-angle scattering function $S(q)$, which is related to the Fourier transform of $g(r)-1$, are calculated for the resulting gel structure which is made of connected fractal clusters. In addition to the short-range features already described in a previous paper, it is found that $g(r)$ goes through a minimum before tending to unity for large r values. As a consequence the scattering function $S(q)$ exhibits a maximum at small q values. After multiplying $S(q)$ by the form factor $P(q)$, the intensity curve $I(q)$ is calculated and its behavior is found to be in good agreement with small-angle neutron-scattering experiments on silica aerogels of various densities. In contrast with previous approaches, the low-q maximum in the $I(q)$ curve is here directly quantitatively accounted for, without introducing any phenomenological *ad hoc* term to describe the intercluster correlations.

I. INTRODUCTION

Silica aerogels are known to be good examples of fractal materials. A revealed by small-angle x-ray-scattering (SAXS) or small-angle neutron-scattering (SANS) experiments,[1-3] they are made of a disordered, but homogeneous, array of connected fractal clusters resulting from the aggregation of primary particles.[4] The analysis of the wave-vector dependence of the scattering intensity $I(q)$ has permitted the determination of two characteristic length scales which are the average size a of the particles and the average size ξ of the clusters. Three distinct domains of wave vectors can be identified. At large q ($q > a^{-1}$), the scattering is dominated by the density fluctuations associated with the particle surface so that, for smooth particles, $I(q)$ follows the Porod law, $I(q) \sim q^{-4}$.[5] At intermediate values of q, for $\xi^{-1} < q < a^{-1}$, the fractal nature of intracluster particle correlations is revealed by a power-law behavior $I(q) \sim q^{-D}$, where D is the fractal dimension[6] of the clusters. Finally, at small q values, for $q \ll \xi^{-1}$, the scattering intensity saturates and eventually decreases as q tends to zero.

Since the range of wave vectors of the fractal regime may often be narrow, it is interesting to have quantitative information about the full $I(q)$ curve. In a previous paper,[7] hereafter referred to as Paper I, we have focused on the crossover between the fractal regime and the Porod regime. From a numerical calculation of $I(q)$ for simulated fractal aggregates, we were able to fully take care of the short-range correlations between the particles constituting the clusters. However, such a calculation cannot simply be extended to describe the long-range intercluster correlations. As far as long-range properties are concerned, the single-aggregate approach is only valid for extremely diluted solutions of aggregated particles where the mean interaggregate distance l is much larger than the mean radius of gyration R of the aggregates. Otherwise, the theoretical $I(q)$ curve of a single aggregate, which saturates for q values smaller than R^{-1}, in the so-called Guinier regime,[5] is no longer valid down to q values of order l^{-1}, where interaggregate correlations start to have some influence. In fact, if one neglects other scattering contributions such as scattering by thermally activated fluctuations, $I(q)$ should vanish for $q < l^{-1}$, since, for distances larger than l, the system becomes homogeneous and should no longer scatter the incident beam. Such behavior cannot be avoided in the case of aerogels were l and R are of the same order of magnitude and should be replaced by ξ. If the experiments can be performed down to sufficiently small q values, if no other artifactual inhomogeneities are present and if scattering by thermal fluctuations is small enough, all the experimental $I(q)$ curves for gels or aerogels should exhibit a maximum. In practice, a maximum is observed, or not, depending on the range of q values available. When it exists, this maximum is more or less pronounced depending on preparation conditions (concentration, catalytic pH, etc.).

Several authors have tried to make some quantitative fit of $I(q)$ in the intermediate- and low-q regime for aerogels or similar gel systems. Some of them[8,9] have used a formula due to Fisher and Burford[10] (see below formula 22) in which ξ plays the role of a radius of gyration. Many others[2,3,11,12] have used a semiempirical formula obtained by introducing a cutoff function to limitate the fractal scaling, in which ξ enters as a correlation length (see below, formula 24). In all cases, these approaches do not take into account the intercluster interactions which give rise to a maximum in the $I(q)$ curves. Recently, Posselt, Pedersen, and Mortensen[13] have addressed this problem by introducing a hard-sphere model to describe

the packing of the connected clusters.

In this paper we present quantitative results for the location and shape of the maximum of the $I(q)$ curve from numerical simulations of the full aerogel structure. This work can be considered as a continuation and improvement of the work reported in Paper I.[7] To model the aerogel, we use here the diffusion-limited cluster-cluster aggregation model (DLCA) in a box[4,14,15] with a sufficiently large initial concentration, rather than the hierarchical model[16] which is only able to build a single aggregate. The difference is that the correlation function $g(r)$, instead of tending to zero for $r \to \infty$, tends to a constant value, which can be taken equal to 1 after a proper normalization. Intercluster correlations are revealed by the presence of a minimum of $g(r)$. The location of this minimum allows one to estimate the mean cluster size ξ. As a consequence, the small-angle scattering function $S(q)$, which is related to the Fourier transform of $g(r)-1$, exhibits a maximum, whose location depends on the concentration. We show that these results are in good agreement with SANS experiments on silica aerogels and we are able to present some quantitative fits with only two adjustable parameters.

In Sec. II, we describe the numerical simulations of gel formation. In Secs. III and IV, we give the results of the calculations for $g(r)$ and $S(q)$, respectively. In Sec. V we compare our numerical results with experiments. In Sec. VI we present a discussion about the physical meaning of the correlation length and in Sec. VII we give a conclusion.

II. NUMERICAL SIMULATIONS OF GEL FORMATION

We have considered a three-dimensional off-lattice extension of the original cluster-cluster model[14,15] in the case of a sufficiently large particle concentration to get a gelling network at the end of the aggregation process. Such a model was first proposed by Kolb and Herrmann[17] to describe the formation of gels, but, at this time, they were considering a two-dimensional model on a lattice.

Initially, identical spherical particles of unit diameter are randomly disposed in a cubic box of edge length L (here L is not necessarily an integer) using a standard sequential addition procedure: attempts are made to center particles, one after another, at points whose coordinates are random numbers uniformly distributed between 0 and L. If a particle overlaps a previous one, it is discarded and a new trial is made. If the process generates N particles, the dimensionless concentration, or volume fraction, c is given by

$$c=\frac{\pi}{6}\frac{N}{L^3} . \tag{1}$$

From previous studies,[18] it is known that, with this procedure, c cannot exceed an upper limit which is called the "jamming concentration," $c_j=0.385$.

Let us consider the starting configuration as a collection of aggregates containing one particle each. At a later time, one obtains a collection of N_a aggregates, the ith aggregate containing n_i particles, so that

$$\sum_{i=1}^{N_a} n_i = N . \tag{2}$$

The algorithm proceeds as follows. An aggregate i is chosen at random according to a probability p_{n_i} which depends on the number of particles n_i that it contains, given by

$$p_{n_i}=\frac{n_i^{\alpha}}{\sum_i n_i^{\alpha}} . \tag{3}$$

In most of our simulations, we have taken $\alpha=-0.55$, a value close to $-1/D$, where $D\simeq 1.78$ is the fractal dimension of the resulting aggregates built in three dimensions (3D),[19] in order to insure that the diffusion coefficient of the aggregates varies with the inverse of their radius. However, in some of our simulations we have varied α for a reason that will be explained later. Then a space direction is chosen at random among the six directions $\pm 1, \pm 1, \pm 1$ and an attempt is made to move the cluster by a step of one unit length in that direction (note that this choice corresponds to performing a random translational Brownian motion on a lattice but, since the original coordinates of the particles are not integers, the aggregates themselves are built off lattice). If the cluster does not collide with any other cluster during this motion, the displacement is performed and the algorithm goes on by choosing again a cluster at random, etc. If instead a collision occurs, the cluster is translated in the chosen direction by the shortest distance ensuring that one of its particles becomes tangent to one particle of the colliding cluster. Then the collection of clusters is updated: the two colliding clusters are discarded and a new cluster, formed by sticking together the colliding clusters, is added to the collection. After that, one cluster is chosen at random, etc. Periodic boundary conditions are used at the edges of the box. The process is stopped when a single aggregate is reached. If the concentration is larger than a characteristic gel concentration c_g, the final aggregates spans the box from edge to edge in the three space directions. This is the usual convention to define a gel network.

A series of calculations has been done to determine the gel concentration c_g as a function of the box size L. In practice we have varied the concentration and we have performed 20 independent runs for each concentration. The gel concentration has been defined as being the concentration at which ten runs end up with a gel. The results are given in Fig. 1 as a log-log plot of c_g versus L. As already found by Kolb and Herrmann,[17] the gel concentration tends to zero in the infinite-L asymptotic limit. Since, at the gelling threshold, an aggregate of fractal dimension D reaches the size L of the box, one should have

$$c_g \sim \frac{L^D}{L^3} \sim L^{-(3-D)} . \tag{4}$$

Our data are well fitted with the slope -1.28 ± 0.05, giving $D\simeq 1.72\pm 0.05$, a value slightly smaller but quite close to the fractal dimension $D=1.78$ of DLCA in three dimensions.[19] Note that we do not recover here a larger

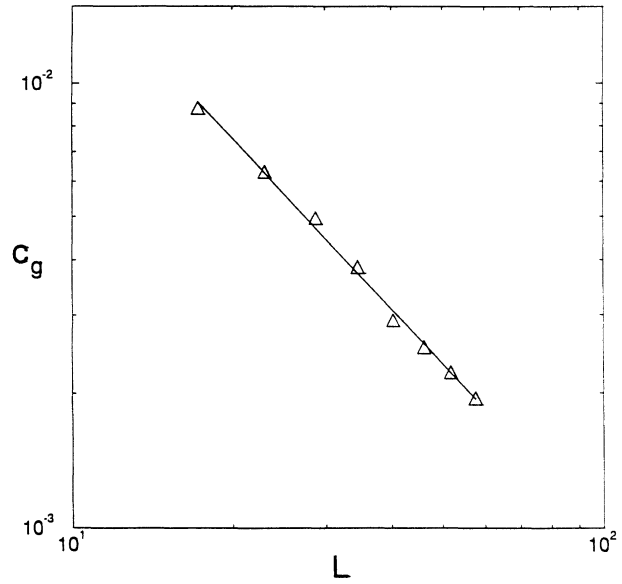

FIG. 1. Log-log plot of the gel concentration c_g as a function of the box size L. The fit by a straight line is shown which gives a slope of -1.28 ± 0.05.

fractal dimension at the gelling threshold as Kolb and Herrmann found in two dimensions.[17] We do not know the reason for such discrepancy (this might be due to the fact that we work off lattice here and that we are limited by the geometrical "jamming" effect rather than by lattice percolation).

In all the calculations reported below, we have considered c values much larger than c_g, in order to get a gel far above the gelling threshold and to be sure that the correlation length ξ is smaller than the box size L. Typical examples of gel networks for two different concentrations are depicted in Fig. 2 where we have visualized a two-dimensional projection of a slice of the box. The slice thickness has been chosen to be proportional to $1/c$ in order to get the same mean coverage in projection. Thus the only difference between the two pictures is in the way the apparent local densities deviate from the mean. As one sees larger holes in case (a), it is apparent that the mean cluster size is larger in that case where the concentration is smaller than in case (b).

III. CALCULATION OF THE CORRELATION FUNCTION $g(r)$

As usual the two-point correlation function $g(\mathbf{r})$ is defined such that $g(\mathbf{r})d^3r$ is proportional to the probability of finding a particle center in a volume d^3r at a distance $\mathbf{r}$ from a given particle center. Consequently, for an isotropic material, the number of particle centers dn located between r and $r+dr$ from a given particle center is proportional to $g(r)4\pi r^2dr$. Knowing from Eq. (1) that, in average, the number of particle centers per unit volume is $6c/\pi$, one can normalize $g(r)$ to unity when r tends to infinity, by writing

$$dn=\frac{6c}{\pi}g(r)4\pi r^2dr=24cg(r)r^2dr\ . \tag{5}$$

We have used this formula to compute $g(r)$ in the gels resulting from our simulations. For each particle in the box, we have counted the number of particle centers located between spheres of radius r and $r+\delta r$, taking care of the periodic boundary conditions when investigating regions outside of the box. Then we have averaged the result over all the N particles in the box and divided it by $24cr^2\delta r$. Moreover, $g(r)$, obtained that way, has been averaged over a large number of independent simulations.

A typical $g(r)$ curve is shown in Fig. 3. It results from an average over 20 simulations with $L=57.7$ and $c=0.05$. Due to the large number of averages made, the curve is less noisy than the $f(r)$ curves reported in Paper I and the short-range features are more clearly revealed. Not only does one see the peak at $r=1$ and the discontinuity at $r=2$ but also one can observe a weaker singularity at

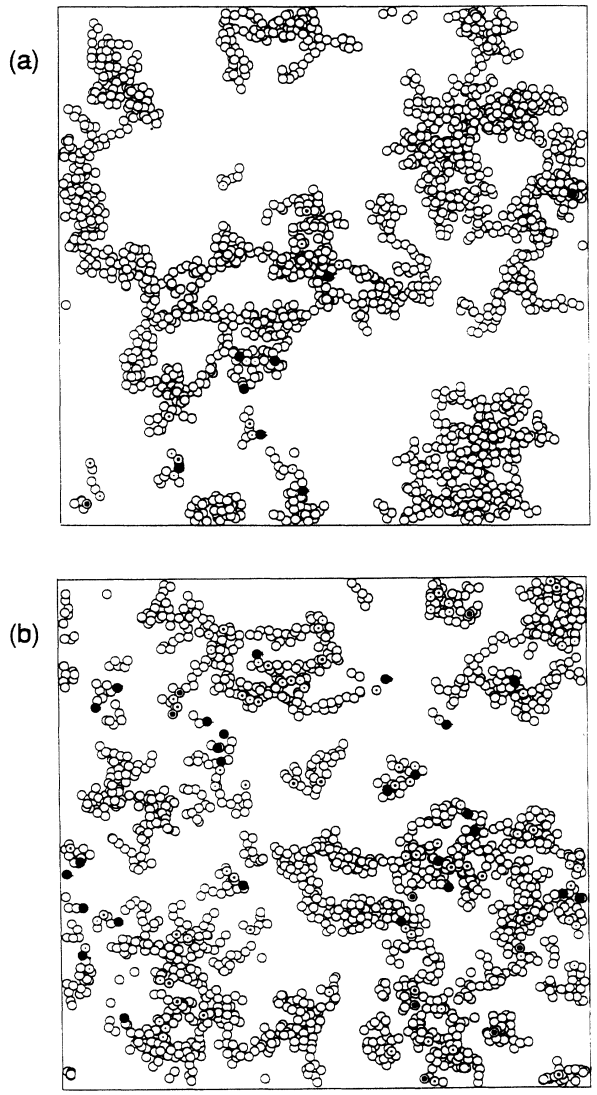

FIG. 2. Two-dimensional projections of the particles contained in a slice of thickness l after obtaining a gel in a box of size $L=57.7$. Cases (a) and (b) corresponds to $c=0.0095$, $l=34.6$ and $c=0.038$, $l=8.65$, respectively. Cross sections of particles that are cut by the front slice edge are shown in black.

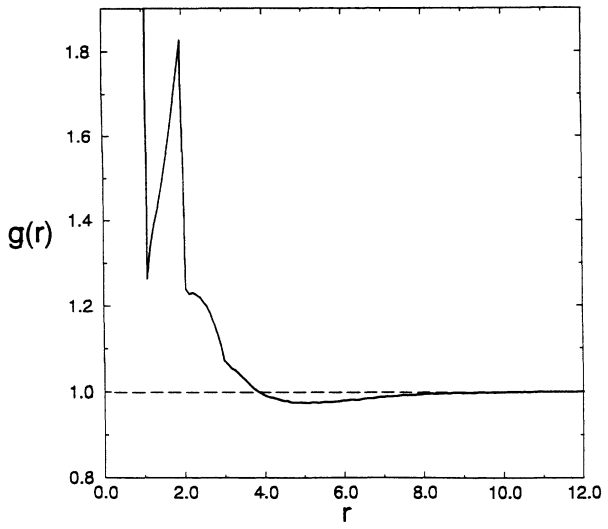

FIG. 3. Plot of $g(r)$ versus r for $L=57.7$ and $c=0.05$. This curve results from an average over 20 simulations.

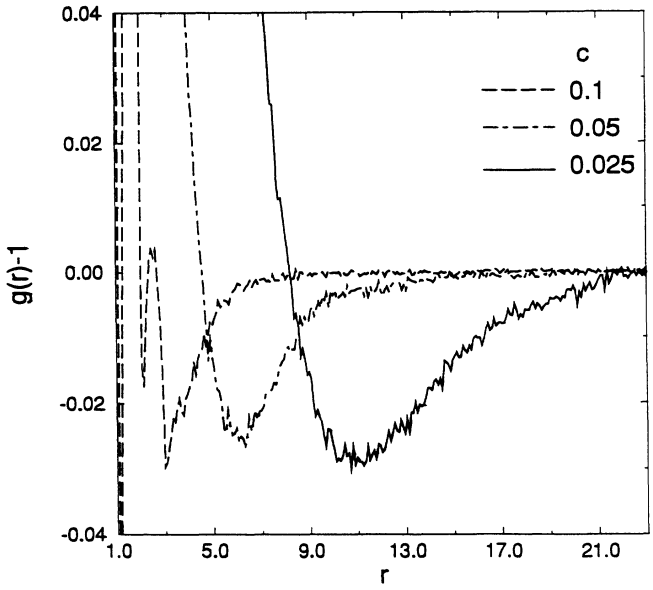

FIG. 4. Plots of $g(r)-1$ versus r for $L=57.7$ and different c values, $c=0.025,0.05,0.1$. These curves result from averages over 30, 20, and 20 simulations, respectively.

$r=3$ (discontinuity of the derivative) which can be explained by analyzing distances between spheres tangent to each sphere of a dimer in a manner very similar to what we did in Paper I to explain the discontinuity at $r=2$. After that, $g(r)$ behaves differently than in Paper I. It goes through a minimum and becomes very close to 1 in a large range of r values. But other features appear for larger r values outside the range of Fig. 3: $g(r)$ goes through a maximum around $r=L$ due to correlations between a given particle and the images of its local environment translated by L in the six directions $\pm1,\pm1,\pm1$. This is an artifact due to the periodic boundary conditions. However, for c values far above c_g, we have identified a sufficiently large range of r values near $r=L/2$ where $g(r)$ stays equal to 1 with a very good precision.

In Fig. 4, we show the $g(r)$ curves obtained for $L=57.7$ and different c values by emphasizing the region near the minimum. One can see that the location of the minimum strongly depends on c. The minimum corresponds to distances between particles located at the periphery of the clusters, where the local density is smaller. Therefore the value of r at the minimum gives a good estimate of the mean cluster size. We will try to be more precise about the cluster geometry in the discussion of Sec. VI, but, since we have found a characteristic length, let us call it ξ.

The dependence of ξ on c is reported in the log-log plot of Fig. 5. Assuming that the clusters are fractal with fractal dimension D, one should get

$$\xi \sim c^{-1/(3-D)} . \tag{6}$$

The value $\xi=3$ reported for the largest concentration $c=0.1$ should be considered as artifactual since for such a concentration the minimum of $g(r)$ sticks on the singularity at $r=3$, as seen in Fig. 4. A straight-line fit of the remaining points for the largest box size gives a slope of -0.77 ± 0.03, leading to $D=1.70\pm0.06$, again slightly smaller but quite close to the fractal dimension $D=1.78$ of 3D DLCA aggregates. The discrepancy can be explained by corrections to scaling since our values of ξ correspond to quite small aggregates.

IV. CALCULATION OF THE SCATTERING FUNCTION $S(q)$

From the single-scattering theory, the scattering function $S(q)$ of a macroscopic system containing identical particles with mean volume fraction c is given by[20]

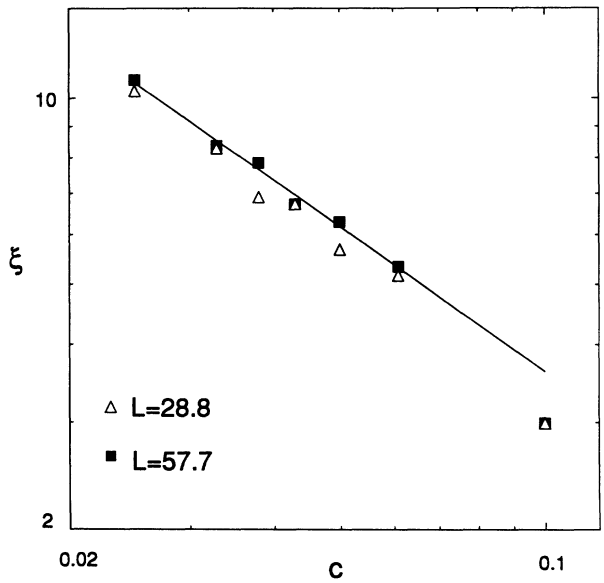

FIG. 5. Log-log plot of ξ, location of the minimum of $g(r)$ versus c, for $L=28.8$ and $L=57.7$. The fit by a straight line of the $L=57.7$ data, excluding the $c=0.1$ point, is shown, giving a slope of -0.77 ± 0.03.

$$S(q)=1+\frac{6c}{\pi}\int_0^\infty [g(r)-1]\frac{\sin qr}{qr}4\pi r^2 dr \ . \tag{7}$$

The infinite boundary of the integral means that the incident beam is scattered by the particles located within the whole macroscopic volume. This formula can be considered as an extension to a large system of formula (20) of Paper I, since the distance distribution function $f(r)$ (with the normalization used in Paper I), is here equal to $(3c/\pi)g(r)$. However, there is an essential difference, which is the presence of $g(r)-1$ instead of $g(r)$. This is due to the fact that, to obtain formula (7), one has subtracted the intensity scattered by a quasi-infinite homogeneous object having the same boundaries as the macroscopic system considered. As a consequence, the formula (7), $S(q)\to 0$ when $q\to 0$ (because the $q\simeq 0$ contribution of the boundaries has been suppressed). Quantitatively, this $q=0$ limit results from the following sum rules:

$$\frac{6c}{\pi}\int_0^\infty g(r)4\pi r^2 dr=\mathfrak{N}-1 \ , \tag{8a}$$

$$\frac{6c}{\pi}\int_0^\infty 4\pi r^2 dr=\mathfrak{N} \ , \tag{8b}$$

where $\mathfrak{N}$ is the total number of particles contained in the macroscopic volume.

When applying formula (7) to real systems, it should be remembered that the underlying theory considers only the single scattering by static (quenched) particles. Therefore the scattering by thermally activated (and correlated) motions of these particles is not considered. It is known that, in the case of liquids, the latter contribution (which there corresponds to scattering by thermally activated density fluctuations) gives a nonzero contribution at $q=0$ proportional to the product of temperature, bulk density, and isothermal compressibility.[21] Since in the following, the formula will be applied to solid aerogels, of lower compressibility than the usual liquids, we will assume that such a contribution is negligible.

In practice, we have calculated $S(q)$ numerically from the preceding $g(r)$ results, by replacing formula (7) by

$$S(q)=1+\frac{6c}{\pi}\int_0^{r_m} [g(r)-g_0]\frac{\sin qr}{qr}4\pi r^2 dr \ . \tag{9a}$$

Here, g_0 is a parameter which is very close, but not strictly equal, to 1, r_m is an upper cutoff, and the integral is computed numerically as a discrete sum. We have chosen $r_m=L/2$, to avoid the boundary artifact mentioned above, but also we have averaged $g(r)$ over many simulations and we have limited ourselves to concentrations sufficiently greater than the gel concentration to obtain a significant range of r values below r_m where $g(r)\simeq 1$. Nevertheless, the truncation of the integral implies that the numerical results for $S(q)$ become meaningless for q values smaller than

$$q_{\min}=\frac{\pi}{r_m} \tag{9b}$$

and, indeed, we have observed that for $q<q_{\min}$ the precise shape of the computed $S(q)$ curve depends on both r_m and g_0. To avoid this problem, we have forced the sum rules (8a) and (8b) to be obeyed, and, instead of using $g_0=1$, we have computed this parameter from

$$g_0=\frac{\int_0^{r_m} g(r)4\pi r^2 dr+\pi/6c}{\int_0^{r_m} 4\pi r^2 dr} \ , \tag{10}$$

where, to compute the integrals, we have used the same discretization as in formula (9a). We have checked that g_0 is always equal to 1 within less that 0.001; however, using (10) instead of $g_0=1$ ensures that $S(q)\to 0$ exactly when $q\to 0$. This trick, which allows one to obtain a continuation of $S(q)$ below $q_{\min}$, is expected to give a reasonably correct result if, in the corresponding infinite system, $g(r)$ is supposed to stay constant for $r>r_m$. This has been checked *a posteriori* by verifying that the numerical results are the same (within the numerical uncertainties) for different L values.

Typical $S(q)$ curves are reported in Fig. 6 for different concentrations and for $L=57.7$. The location of $q_{\min}$ is indicated by the arrow. All the curves exhibit the same damped oscillations at large q, characteristic of short-range correlations, which were already described in Paper I. The linear fractal regime is quite narrow and is more extended for low concentrations. It corresponds to a fractal dimension $D\simeq 1.75$, as expected. In view of the smallness of the clusters, it is quite remarkable that the slope gives the right fractal dimension. However, for the largest concentration $c=0.1$, it is hard to define a fractal regime even if, accidentally, the apparent slope is close to -1.75 near the inflexion point. At lower q values, all the curves exhibit a maximum. The location of the maximum, q_m, as well as the intensity of the maximum, $S(q_m)$, have been reported as a function of c in Table I together with the corresponding values of ξ. If one for-

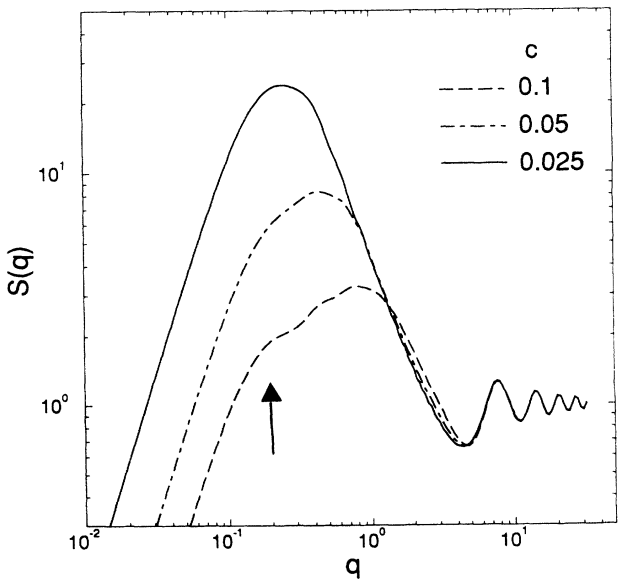

FIG. 6. Log-log plot of $S(q)$ versus q for $L=57.7$ and different c values. The parameters are the same as in Fig. 4. Here and in the following figures the location of $q_{\min}$ is indicated by the arrow.

TABLE I. For each concentration c considered in the simulations, we have reported the location ξ of the minimum of $g(r)$, the location q_m of the maximum of $S(q)$, the product $q_m\xi$, the intensity of the maximum $S(q_m)$ the ratio $S(q_m)/c\xi^3$, the characteristic length ζ entering the low-q expansion of $S(q)$, and the ratio ζ/ξ. We recall that q is here a dimensionless quantity which is, in fact, equal to $2Qr_0$ where Q is the dimensioned wave vector and r_0 is the radius of the primary particles, and also that $S(q)$ has been normalized to unity for large q.

c	ξ	q_m	$q_m\xi$	$S(q_m)$	$\frac{S(q_m)}{c\xi^3}$	ζ	$\frac{\zeta}{\xi}$
0.025	10.7	0.26	2.78	24.7	0.81	38.5	3.6
0.033	8.4	0.31	2.60	16.0	0.82	28.1	3.3
0.038	7.8	0.37	2.88	12.8	0.71	25.9	3.3
0.043	6.7	0.40	2.68	10.5	0.81	21.0	3.1
0.050	6.3	0.43	2.71	8.3	0.66	18.4	2.9
0.061	5.3	0.52	2.76	6.2	0.68	15.5	2.9
0.100	3.0	0.80	2.40	3.3	1.22	10.0	3.3

gets the artifactual situation $c=0.1$, the product $q_m\xi$ is almost constant, so that one has approximately

$$q_m \simeq \frac{2.75}{\xi} . \tag{11}$$

On the other hand, one observes that the intensity of the maximum $S(q_m)$ is roughly proportional to $c\xi^3$, which is the number of particles contained in a sphere of diameter ξ:

$$S(q_m) \simeq 0.75 c\xi^3 . \tag{12}$$

For very low q values (smaller than q_m) we get a linear behavior with slope $+2$. This is consistent with the low-q expansion of formula (7), which predicts

$$S(q) \simeq \zeta^2 q^2 , \tag{13a}$$

with

$$\zeta^2 = \frac{6c}{\pi} \int_0^{r_m} [g_0 - g(r)] 4\pi r^4 dr . \tag{13b}$$

This result is derived from a Taylor expansion of $\sin qr/qr$ inside the integral of (7). Note that, for an infinite system (where $r_m = \infty$ and $g_0 = 1$), such a procedure is mathematically justified if $g(r)-1$ tends to zero more quickly than any power law when r tends to infinity. Our numerical results, which lead to a quite size-independent result for ζ, strongly support a large-r exponential decay for $g(r)-1$. This defines another characteristic length ζ which can be usefully compared to ξ. In Table I, we have reported the numerical estimates of ζ from our computed $S(q)$ curves for the different c values considered. We find that ζ is roughly proportional to ξ.

It is instructive to compare the present $S(q)$ curves for gels with the corresponding curves for isolated aggregates. Such a comparison is done in Fig. 7, where we compare the $S(q)$ curve for $c=0.025$ with the ones obtained with the hierarchical model for aggregates containing $n=32$ and 64 particles. As expected, the three curves are superimposed in the high-q regime as well as

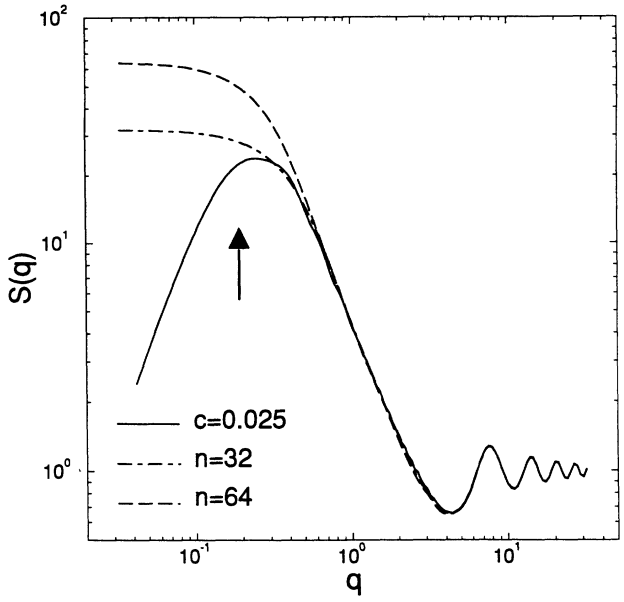

FIG. 7. Comparison between the $S(q)$ curve for a gel with $c=0.025$ and $S(q)$ curves calculated with the hierarchical model for aggregates containing $n=32$ and 64 particles.

in the fractal regime; the difference occurs at low q when one starts to investigate correlations between particles in the "active" region, i.e., near the external surface in the case of an isolated aggregate, or in the intercluster region in the case of a gel. Since the structure of the connected clusters results from sticking of aggregates, neighboring connected clusters can be viewed as interpenetrating aggregates. Therefore the deviations to the fractal regime at low q should be almost the same for the $S(q)$ curve of the cluster and for the one of the corresponding isolated aggregate, and the differences should occur only slightly above the location of the maximum of the gel curve. Therefore the number of particles per cluster can be estimated by fitting at best the whole gel curve after the maximum with the curve of a single aggregate containing n particles. Here, in the case $c=0.025$ one can estimate that the mean number of particles in a cluster is between 32 and 64. This estimate is greater than the number $c\xi^3$ calculated above. We will come back to this in the discussion of Sec. VI.

As should be expected, the characteristics of the maximum of $S(q)$ do not depend only on the mean cluster size ξ, but also on the extension of the cluster size distribution. The cluster size distribution is reminiscent of the size distribution of the aggregates observed during the aggregation process and therefore it strongly depends on the nature of the aggregation mechanism. As a consequence, all the quantitative analysis done above, as well as the values of the constants appearing in formulas (11) and (12), are only valid for DLCA where it is known that the aggregate size distribution presents a well-defined maximum. A simple way to check that is to vary the kinetic exponent α appearing in formula (3). It is known that, if α does not become larger than a threshold value $\alpha_c \simeq 0.5$, the fractal dimension of the aggregates does not depend too much on α, but the shape of their size distri-

bution changes.[4,22] For α large and negative, the distribution is quasimonodisperse while, when α increases, polydispersity increases. In Fig. 8, we give the $S(q)$ curves obtained for three values of α. As expected, the maximum is sharper for α large and negative and broader for the positive $\alpha=0.1$ value. We have observed that, for large α values, another sharp peak appears, which corresponds to a breakdown in the cluster size distribution announcing the transition to particle-cluster aggregation at α_c.[4,22]

V. SCATTERING INTENSITY AND COMPARISONS WITH EXPERIMENTS

To better compare with experiments, we have computed the theoretical $I(q)$ curve by using

$$I(q)=S(q)P(q)\ , \tag{14}$$

where $P(q)$ is the normalized form factor for spherical particles of unit diameter:

$$P(q)=\left[24\frac{\sin q/2-(q/2)\cos q/2}{q^3}\right]^2 . \tag{15}$$

The log-log plots of $I(q)$ versus q for different concentrations are reported in Fig. 9. As a result of the multiplication by $P(q)$ and the use of the logarithmic scale, the maximum appears to be relatively less pronounced than in the $S(q)$ curves.

Before comparing with experiments, we recall that our group has performed several SANS experiments on different kinds of silica aerogels that are called "colloidal" and "polymeric" aerogels.[3,23,24] The colloidal aerogels,[23] which are synthesized from a silica sol, are made of quasimonodisperse spherical particles whose size can be determined directly on a micrograph. The polymeric aerogels instead are prepared by chemical reactions (hydrolysis and condensation) of organosilicates. According to the pH value of the hydrolysis aqueous solution, we can distinguish "basic" and "neutral" aerogels. The basic aerogels[24] are made of larger-sized, but strongly polydisperse, primary particles while, for the neutral aerogels,[3] particle sizes are smaller and extend down to the atomic scale. According to previous studies,[3,23,24] only colloidal and basic aerogels can be considered as grown according to DLCA while the neutral aerogels are more likely grown according to the chemically limited cluster-cluster aggregation process.[4,25]

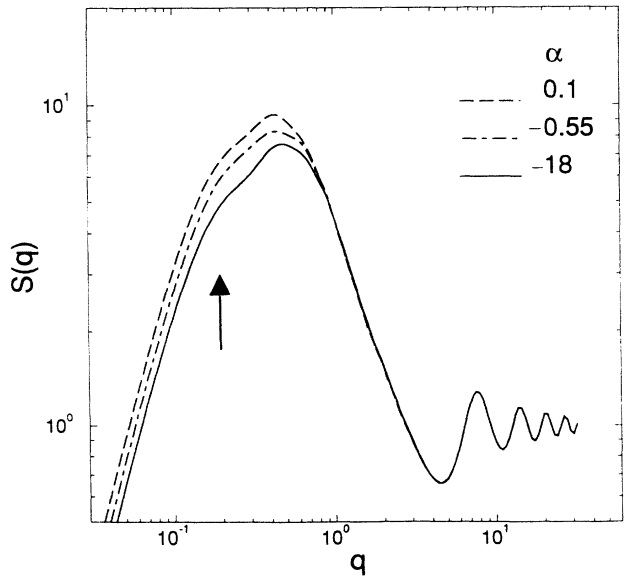

FIG. 8. Log-lot plot of $S(q)$ versus q for $L=57.7$, $c=0.05$, and different α values, $\alpha=0.1, -0.55, -18$. These curves result from averages over 50, 20, and 40 simulations, respectively.

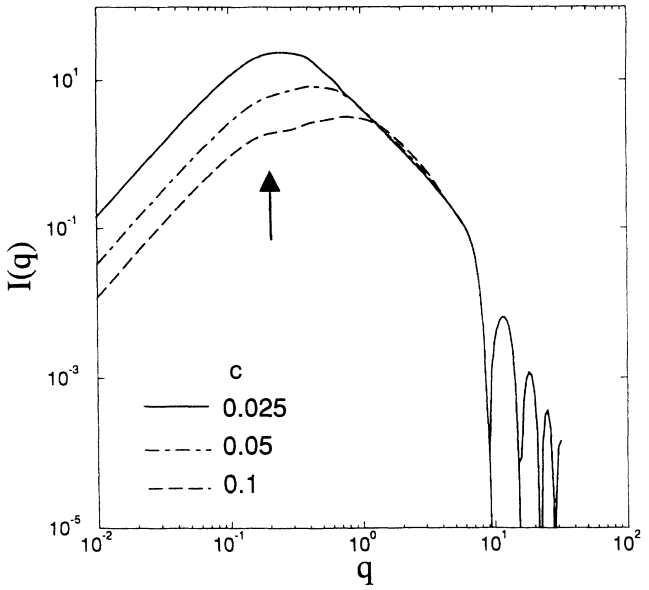

FIG. 9. Log-log plot of the scattering intensity curve $I(q)$ versus q for different c values. The parameters are the same as in Fig. 4.

Three experimental $I(q)$ curves for basic aerogels with different densities are shown in Fig. 10. Both the Porod regimes and the fractal regimes are nicely superimposed, indicating that the mean average size of the primary particles is the same for the three samples, as well as the fractal dimension of the clusters. Apart from the absence of large-q oscillations in the Porod region, as a result of the large dispersity in the particle diameters, these $I(q)$ curves behave pretty much as in Fig. 9: the location of the low-q maximum increases with the gel density.

Quantitative fits are reported in Fig. 11. The concentrations that we have used for the fit are those corresponding to the aerogel density ρ, according to the formula

$$c=\frac{\rho}{\rho_0}\ , \tag{16}$$

where $\rho_0=2.2\ \mathrm{g\,cm^{-3}}$ is the density of silica. The only two adjustable parameters are the mean particle diameter value and a multiplicative constant for the intensity. Note that varying these parameters in a log-log plot does not change the shape of the curve but only leads to translations along the x and y directions. The three fits have been performed together using the same values for

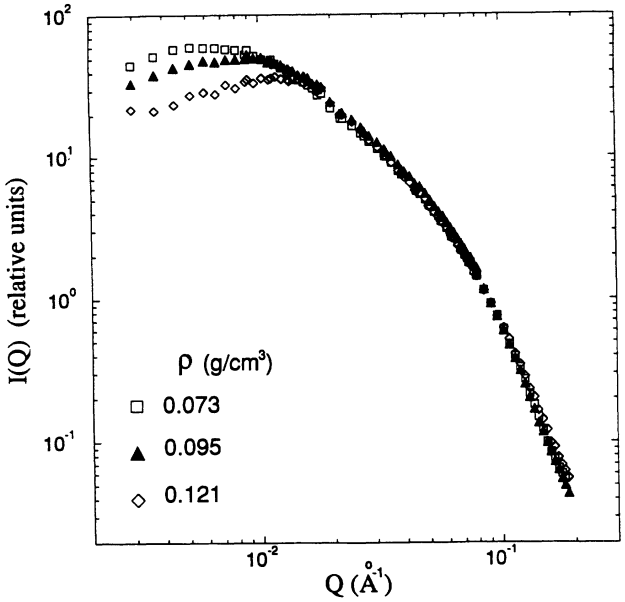

FIG. 10. Log-log plot of the experimental scattering intensity curve $I(Q)$ versus Q for three basic aerogels of the same family, i.e., with different densities ($\rho=0.073$, 0.095, 0.121 g cm^{-3}) but with the same average size of the primary particles.

these parameters. A discrepancy occurs in the Porod region where the experimental curves stay slightly below the maxima of the large-q oscillations of the theoretical curves. Such a discrepancy can be attributed to the strong polydispersity of the primary particles. Preliminary calculations of DLCA with polydisperse particles

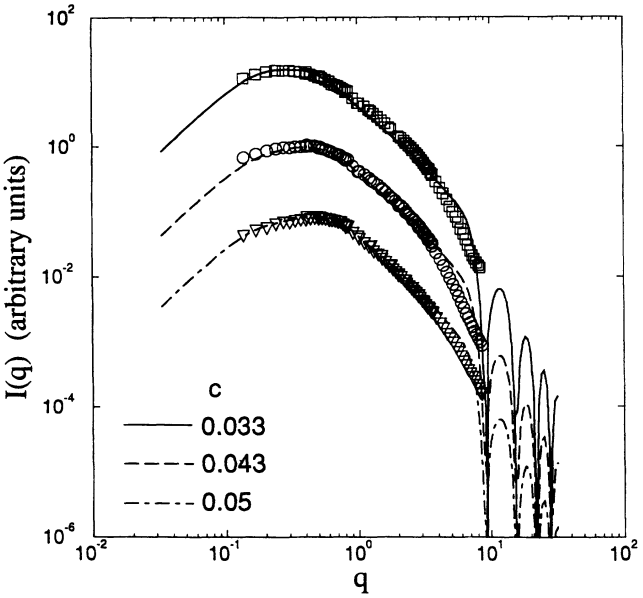

FIG. 11. Comparison between simulations and experiments for three basic aerogels of the same family. The concentrations used in the simulations $c=0.033,0.043,0.05$ are calculated from the aerogel densities ($\rho=0.073,0.095,0.110$ g cm^{-3}) using formula (12). The two adjustable parameters, which are a multiplicative constant for the intensity and the particle diameter, taken to be 46 Å, are the same for the three curves. The curves have been arbitrarily shifted vertically for clarity.

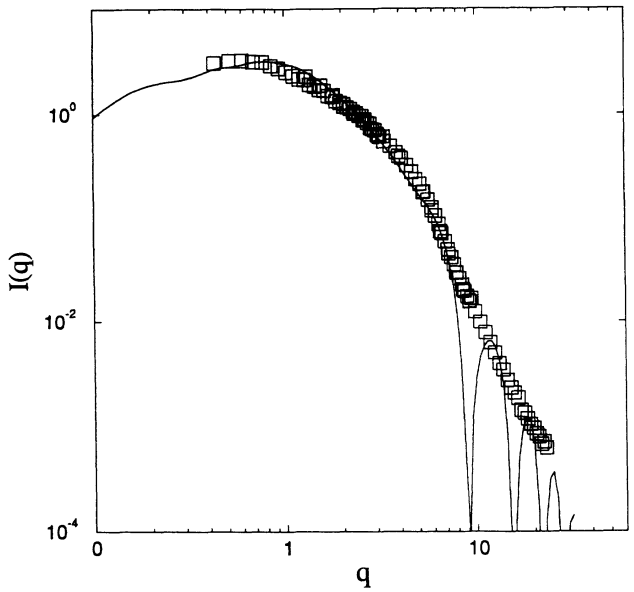

FIG. 12. Comparison between a simulation and an experiment in the case of a colloidal aerogel for which both the density and the diameter of the primary particles are known. The concentration is $c=0.1$. The only adjustable parameter here is the multiplicative constant for the intensity.

(which will be published elsewhere[26]) indicate that, for very large polydispersities, not only are the Porod oscillations washed out but also the entire curve is shifted towards lower q values.

Another fit is reported in Fig. 12 for a colloidal aerogel. Here the particle diameter is known. Therefore the fit has been obtained with only one adjustable parameter which is the multiplicative constant for the intensity (corresponding to a vertical translation of the curve). Here the polydispersity is smaller and therefore the experimental curve goes through the maxima of the oscillations in the Porod region. However, small discrepancies occur at low q values in this fit as well as in the fits of Fig. 11. It seems that the theoretical maximum is systematically a bit sharper than in the experiments. We might invoke some approximations of our DLCA model which neglects rotational diffusion, aggregate deformations, as well as all kinds of restructuring effects. In Paper I, we have shown that large restructuring is certainly not present, at least in the early stages of the aggregation process. However, in the last stages, when the gel structure is under formation, the diffusion process loses its leading character and it might be that restructuring and rotational motions have some influence on the gel structure and the intercluster correlations.

VI. DISCUSSION ABOUT THE CORRELATION LENGTH AND THE CLUSTER STRUCTURE

Since, in the past, many authors have given estimates not only for the fractal dimension D but also for the correlation length ξ by fitting the experimental $I(q)$ curves for gels or aerogels, we think it might be useful to make more precise the meaning of ξ in our approach and to compare with previous investigations.

As introduced in Sec. III, ξ is defined here as the minimum of the $g(r)$ curve. The large r behavior of $g(r)$ is characteristic of intercluster correlations. Since the disordered array of clusters is like an amorphous structure, its correlation function should tend to unity with damped oscillations as r tends to infinity. However, due to the strong disorder and the cluster size polydispersity, these oscillations are highly damped and here one can only detect the first minimum. Knowing that for a disordered sphere packing of diameter σ, the first minimum of $g(r)$ is always located just above the δ peak at $r=\sigma$, one can deduce that our ξ is only slightly larger than what we will call a mean "hard-sphere" diameter σ of the clusters, which can also be defined as the mean distance between the centers of two neighboring connected clusters. If we remember that the connection between two neighboring clusters results from the last stages of the DLCA process, i.e., from the sticking of two fractal aggregates of almost the same radius of gyration R, one can relate σ and R by

$$\frac{\sigma}{R}=2\sqrt{4^{1/D}-1}\ . \tag{17}$$

This relation, which has been established rigorously in the hierarchical model,[27,28] is also quite well verified in the case of the DLCA process in a box. Taking $D=1.70$, which is the effective fractal dimension for small DLCA aggregates containing from 10 to 1000 particles, one gets $R\simeq 0.46\sigma$. Then, using the scaling law

$$n=CR^{D} \tag{18}$$

with $C=4.36$ and $D=1.70$, which are appropriate values for such small DLA clusters, one can obtain an estimate of n, the number of particles in an aggregate of radius of gyration R, which is therefore the mean number of particles per cluster. In Table II, we have listed the values of R and n as a function of c, assuming $\sigma=\xi$ [Table II(a)] or $\sigma=0.85\xi$ [Table II(b)]. Knowing also from previous studies that the mean maximum diameter of a DLCA aggregate is about four times greater than its radius of gyration R, one can check that it is always greater than σ, as a consequence of the Interpenetration between connected neighboring clusters.

TABLE II. (a) For each concentration c considered in the simulations, we have reported the value of the "hard-sphere diameter" σ, here taken equal to ξ, the mean radius of gyration R of the clusters, the mean number of particles per cluster n, the product $c\sigma^3$, and f, the packing fraction of the random packing of hard spheres equivalent to the cluster structure. (b) Same as (a) but with $\sigma=0.85\xi$.

c	σ	R	n	$c\sigma^3$	f
		(a)			
0.025	10.7	4.93	65.8	30.3	0.47
0.033	8.4	3.87	43.6	19.6	0.45
0.038	7.8	3.59	38.4	18.0	0.47
0.043	6.7	3.09	29.7	12.9	0.44
0.050	6.3	2.90	26.7	12.5	0.47
0.061	5.3	2.44	19.9	9.08	0.46
0.100	3.0	1.38	7.57	2.70	0.36
		(b)			
0.025	9.20	4.24	50.9	19.5	0.38
0.033	7.22	3.33	33.7	12.4	0.37
0.038	6.71	3.09	29.7	11.5	0.39
0.043	5.76	2.65	23.0	8.23	0.36
0.050	5.42	2.50	20.7	7.95	0.38
0.061	4.56	2.10	15.4	5.78	0.37
0.100	2.58	1.19	5.86	1.72	0.29

Using the concept of hard-sphere diameter introduced above, the disordered lattice of interpenetrating connected aggregates can be viewed as a random packing of tangent spheres of mean radius σ. One can characterize this packing by its packing fraction f, which is the volume occupied by the spheres divided by the total volume:

$$f=\frac{\pi}{6}\frac{N_c\sigma^3}{V}\ , \tag{19}$$

where N_c is the total number of clusters. Since the total number of particles N in the volume V is related to N_c and the mean number of particles per cluster n by

$$N=nN_c \tag{20}$$

and using relation (1), one gets

$$f=\frac{c\sigma^3}{n}\ . \tag{21}$$

The packing fraction deduced from this formula has been reported in Table II. In the case $\sigma=\xi$, f is of order 0.46, and in the case $\sigma=0.85\xi$, it is of order 0.38. In all cases this is typical of a quite loose random packing. It might not be fortuitous that, for the reasonable choice of σ slightly smaller than ξ, one recovers the packing fraction corresponding to the jamming situation, as if the aggregation process has been stopped when the clusters become so large that they can no longer fill the space, as in a random sequential addition process. In practice, the actual ratio between σ and ξ might be a bit larger since the jamming threshold can be slightly increased due to the cluster size polydispersity. Such reasoning is approximate and it should not be pushed too far. However, it is remarkable that the estimates for n listed in Table II(b) are compatible with the analysis made above when comparing the $S(q)$ curve for a gel directly with single-aggregate curves (Fig. 7).

It should be emphasized that the present approach is completely different than most of the previous ones, which used phenomenological formulas, based on the single-aggregate theory, to fit the experimental results. This difference needs some discussion. Some authors[8,9] have used the Fisher-Burford formula[10]

$$S(q)=S(0)\left[1+\frac{2}{3D}\xi_1^2q^2\right]^{-D/2} \tag{22}$$

with various coefficients in front of the q^2 term. Here we have adopted the coefficient which leads to the following low-q expansion:

$$S(q)=S(0)(1-\tfrac{1}{3}q^2\xi_1^2) \tag{23}$$

so that the Guinier regime is well reproduced if ξ_1 is the

radius of gyration R of the aggregate. In Fig. 13 we have compared our $S(q)$ curve for $c=0.025$ with that given by the above formula using $D=1.70$, $\xi_1=R=4.24$, as taken in Table II(b), and adjusting $S(0)$ to fit the fractal regime at best. A compromise is made near the maximum and only a small part of the linear fractal regime is fitted.

Other authors[2,3,11,12] have used the more sophisticated formula

$$S(q)=1+\frac{D2^D\Gamma(D-1)}{q^D}\frac{\sin[(D-1)\tan^{-1}(q\xi_2)]}{[1+(1/q\xi_2)^2]^{(D-1)/2}}, \quad (24)$$

in which ξ_2 is a phenomenological correlation length introduced in an exponential cutoff function to limit the fractal scaling at large interparticle distances. If one notices that the low-q expansion for this formula leads to

$$S(q)=S(0)\left[1-\frac{D(D+1)}{6}q^2\xi_2^2\right], \quad (25)$$

the value of ξ_2 should correspond to

$$\xi_2=\left[\frac{2}{D(D+1)}R\right]^{1/2}. \quad (26)$$

The apparent improvement of formula (24) compared to formula (22) is that both low-q and large-q deviations from the fractal regime are accounted for and consequently there is one parameter left. In the same Fig. 13 we have represented the curve obtained from this formula using $D=1.70$ and the value of ξ_2 corresponding to $R=4.24$. Not only is the low-q region badly reproduced but also the slope of the fractal regime is erroneous. This comes from the fact that formula (24) reproduces the right slope only when ξ_2 is very large. In practice most of the authors did not make any attempt to fit the large-q regime and they did use this formula to fit the low-q and the fractal regime, as done with the Fisher-Burford formula. Consequently, they replaced formula (20) by

$$S(q)=\frac{S(0)}{q\xi_2}\frac{\sin[(D-1)\tan^{-1}(q\xi_2)]}{[1+(q\xi_2)^2]^{(D-1)/2}}. \quad (27)$$

In practice the $S(q)$ curve obtained with this formula is almost superimposed on the Fisher-Buford curve, if one chooses ξ_2 related to $R=\xi_1$ through Eq. (26). The conclusion is that, if such formulas may give nice results in the diluted cases and can give an estimate of R (if one knows the relation between ξ and R), they are not so useful in the case of gels since the maximum cannot be fitted. Using them to get the fractal dimension does not give improvement compared to a simple fit of the linear regime.

Recently Posselt, Pedersen, and Mortensen[13] have proposed to account for the low-q maximum in the $I(q)$ curve using some phenomenological function to describe the intercluster correlations, assuming that the clusters are arranged as in a random packing of hard spheres (following a reasoning quite close to that developed in the beginning of this section). In their approach $I(q)$ results from the product of $P(q)$ (particle form factor) with $S(q)$ (single-aggregate scattering function), but they consider an extra factor

$$\Phi(q)=\frac{1}{1+p\Theta(\sigma q)} \quad (28a)$$

with

$$\Theta(\sigma q)=3\frac{\sin\sigma q-\sigma q\cos\sigma q}{(\sigma q)^3}. \quad (28b)$$

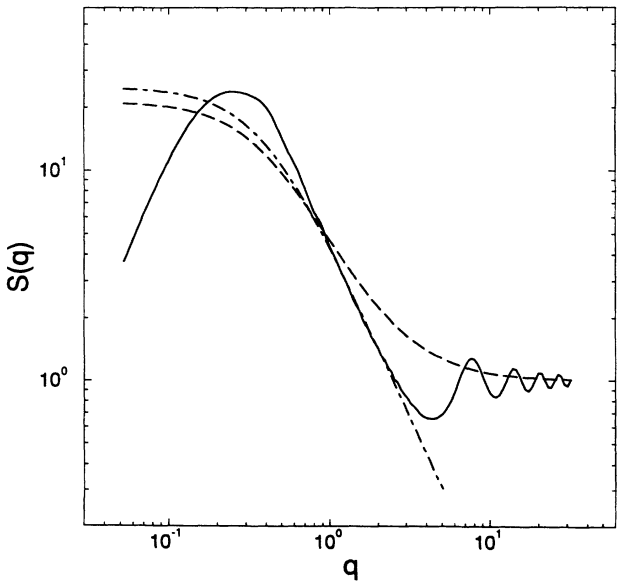

FIG. 13. Comparison of the $S(q)$ curve for $c=0.025$ (solid curve) with the $S(q)$ curves obtained using formula (18) (dot-dashed curve) and formula (20) (dashed curve), as expected in text.

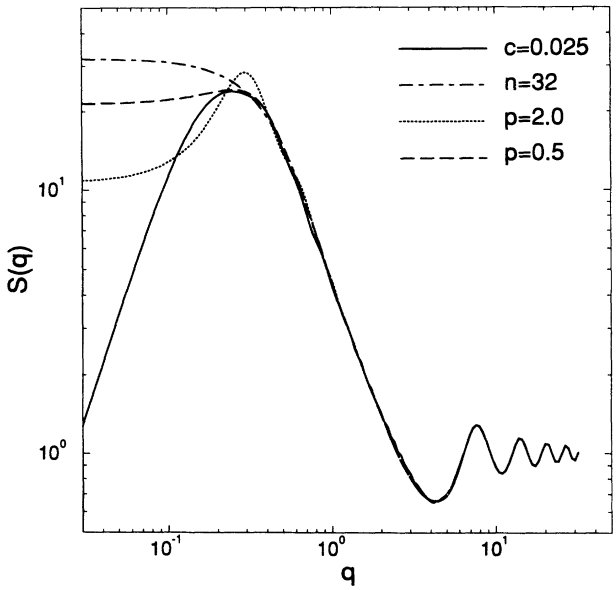

FIG. 14. The solid line corresponds to the $S(q)$ curve for a gel with $c=0.025$. The dash-dotted line corresponds to the $S(q)$ curve for a single aggregate containing 32 particles. The dotted and dashed lines correspond to the curves obtained by multiplying the single-aggregate $S(q)$ curve by the $\Phi(q)$ function of Posselt, Pedersen, and Mortensen (Ref. 13) with $\sigma=18$ and $p=2.0$ and 0.5, respectively.

This function depends on two parameters, σ, which is the cluster mean diameter, and p, which is proportional to what they call the "packing ratio." In Fig. 14, we show two curves obtained when multiplying the $n=32$ single-aggregate $S(q)$ curve by such a $\Phi(q)$ factor with $\sigma=18$ (in particle diameter units) and two different values of p, and we compare with our gel curve for $c=0.025$. The best fit of our maximum is obtained with $p=0.5$ and with larger p values the peak becomes too narrow. Posselt, Pedersen, and Mortensen[13] claim to have used $p\sim4$ to fit their experiments, but it has been discovered that there was an error by a factor of 3 in their definition of p,[29] and therefore the true value of p becomes $p=1.333$, between the two p values used in Fig. 14. Nevertheless, with our best choice ($p=0.5$), only the region close to the maximum is reproduced. At low q, their curve strongly deviates from our gel curve since $\Phi(q)$ saturates to a constant value as q tends to zero. Note also that the value chosen for σ to obtain the best fit is about twice our estimate of the cluster diameter.

VII. CONCLUSION

In this paper we have shown that the presence of a low-q maximum in the experimental $I(q)$ curve for a gel structure made of connected fractal clusters resulting from the DLCA growth process is well accounted for by a direct numerical calculation based on simulation of DLCA in a box. As in the experiments, the location of the maximum increases when increasing the gel density and we have been able to present some reasonable fits of experimental data with only two (or even one) adjustable parameter. We have given (Fig. 9) a series of theoretical $I(q)$ curves for different concentrations which, we hope, will be very useful to fit other experimental curves in the future, at least in the cases where the gels have been grown according to the DLCA process. One advantage of such direct comparison with simulations is that it remains valid for high concentrations (such as $c=0.1$) where the fractal character of the clusters disappears. However, even if we have obtained quite good agreement between simulations and experiments, it should not be forgotten that the DLCA process, as considered here, neglects some important physical processes such as rotational diffusion and restructuring effects. Including restructuring is more difficult here, in a box, than within the hierarchical scheme (as the one used in Paper I), but it is not too hard to include rotational diffusion and we will certainly try to do it in the future. Also, the extension to chemically limited cluster-cluster aggregation (CLCA) is in progress. It is expected that the maximum of $I(q)$ should be broader due to the larger cluster size polydispersity of CLCA compared to the one of DLCA. We also intend to perform DLCA, as well as CLCA, calculations starting with polydisperse spherical particles. Studies of the evolution of the $I(q)$ curve during the aggregation process are also in progress. Finally, in the future, we would like to investigate the order of magnitude of the intensity scattered by thermal fluctuations in aerogels to check if such scattering has no influence on the shape of the maximum of $I(q)$.

ACKNOWLEDGMENTS

We would like to thank Dr. J. S. Pedersen for his deep understanding of our work and for his very interesting and constructive remarks. One of us (A.H.) would like to acknowledge support from CONICIT (Venezuela). Laboratoire de Science des Matériaux Vitreux is Unité de Recherche Associé au CNRS No. 1119.

[1]D. W. Schaefer, J. E. Martin, and K. D. Keefer, Phys. Rev. Lett. **56**, 2199 (1986).
[2]T. Freltoft, J. K. Kjems, and S. Sinha, Phys. Rev. B **33**, 269 (1986).
[3]R. Vacher, T. Woignier, J. Pelous, and E. Courtens, Phys. Rev. B **37**, 6500 (1988).
[4]R. Jullien and R. Botet, *Aggregation and Fractal Aggregates* (World Scientific, Singapore, 1987).
[5]A. Guinier and J. Fournet, *Small Angle Scattering of X-rays* (Wiley-Interscience, New York, 1955).
[6]B. B. Mandelbrot, *Fractals: Form, Chance and Dimension* (Freeman, San Francisco, 1977).
[7]A. Hasmy, M. Foret, J. Pelous, and R. Jullien, Phys. Rev. B **48**, 9345 (1993).
[8]G. Dietler, C. Aubert, D. S. Cannell, and P. Wiltzius, Phys. Rev. Lett. **57**, 3117 (1986).
[9]B. Cabane, M. Dubois, F. Lefaucheux, and M. C. Robert, J. Non-Cryst. Solids **119**, 121 (1990).
[10]M. E. Fisher and R. J. Burford, Phys. Rev. **156**, 583 (1967).
[11]P. Dimon, S. K. Sinha, D. A. Weitz, C. R. Safinya, G. S. Smith, V. A. Varady, and H. M. Lindsay, Phys. Rev. Lett. **57**, 595 (1986).
[12]F. Ferri, B. J. Frisken, and D. S. Cannell, Phys. Rev. Lett. **67**, 3626 (1991).
[13]D. Posselt, J. S. Pedersen, and K. Mortensen, J. Non-Cryst. Solids **145**, 128 (1992).
[14]P. Meakin, Phys. Rev. Lett. **51**, 1119 (1983).
[15]M. Kolb, R. Botet, and R. Jullien, Phys. Rev. Lett. **51**, 1123 (1983).
[16]R. Botet, R. Jullien, and M. Kolb, J. Phys. A **17**, L75 (1983).
[17]M. Kolb and H. Herrmann, J. Phys. A **18**, L435 (1985).
[18]D. W. Cooper, Phys. Rev. A **38**, 522 (1988).
[19]P. Meakin, J. Colloid. Interface Sci. **102**, 491 (1984).
[20]L. A. Feigin and P. I. Svergun, *Structure Analysis by Small Angle X-rays and Neutron Scattering* (Plenum, New York, 987).
[21]P. A. Egelstaff, *An Introduction to the Liquid State* (Academic, London, 1967).
[22]P. Meakin, T. Vicsek, and F. Family, Phys. Rev. A **32**, 1122 (1985).
[23]M. Foret, J. Pelous, and R. Vacher, J. Phys. I (France) **2**, 791 (1992).
[24]R. Vacher, T. Woignier, J. Phalippou, J. Pelous, and E. Courtens, J. Non-Cryst. Solids **106**, 161 (1988).
[25]R. Jullien and M. Kolb, J. Phys. A **17**, (1984).
[26]A. Hasmy, R. Vacher, and R. Jullien, Phys. Rev. B **50**, 1305 (1994).
[27]R. Ball and R. Jullien, J. Phys. (Paris) Lett. **45**, L1031 (1984).
[28]R. Jullien, J. Phys. A **17**, L771 (1984).
[29]D. Posselt (private communication).